Hindawi
Cellular Microbiology
Volume 2024, Article ID 6458900, 17 pages
https://doi.org/10.1155/2024/6458900

Research Article

Three-Dimensional Culture Modelling Reveals Divergent *Mycobacterium tuberculosis* Virulence and Antimicrobial Treatment Response

Magdalena K. Bielecka,[1] **Liku B. Tezera**,[1] **Elena Konstantinopoulou**,[1] **Nicola Casali**,[2] **Orestis L. Katsamenis**,[3] **Ximena Gonzalo**,[2] **Francis Drobniewski**,[2] **and Paul T. Elkington**[1]

[1]*NIHR Biomedical Research Centre, Clinical and Experimental Sciences Academic Unit, Faculty of Medicine, University of Southampton, Southampton, UK*
[2]*Department of Infectious Disease, Imperial College London, London, UK*
[3]*μ-VIS X-ray Imaging Centre, Faculty of Engineering and Physical Sciences, University of Southampton, Southampton, UK*

Correspondence should be addressed to Paul T. Elkington; p.elkington@soton.ac.uk

Received 19 August 2022; Revised 23 March 2023; Accepted 11 March 2024; Published 3 May 2024

Academic Editor: Sanket Kaushik

Copyright © 2024 Magdalena K. Bielecka et al. This is an open access article distributed under the Creative Commons Attribution License, which permits unrestricted use, distribution, and reproduction in any medium, provided the original work is properly cited.

Tuberculosis (TB) remains a persistent epidemic, and the emergence of drug-resistant *Mycobacterium tuberculosis* (Mtb) presents a global healthcare threat. While some new agents have been successfully introduced, innovative technologies to evaluate emerging anti-TB compounds are required to inform transformative approaches. Mtb is an obligate human pathogen, and consequently utilizing models that are consistent with human disease is likely to be critical. We have developed a human 3-dimensional (3-D) cell culture model that reflects human disease gene expression patterns and causes Mtb to become pyrazinamide sensitive *in vitro*. Here, we identify key differences in virulence between the standard laboratory strain, Mtb H37Rv, and clinical isolates. We demonstrate that Mtb H37Rv is attenuated in the 3-D system, more susceptible to antibiotics and hyperinflammatory compared to clinical isolates. Prolonged *in vitro* culture of a clinical strain leads to attenuation. We then characterise antibiotic sensitivity of multi-drug-resistant Mtb within the 3-D model and define relative bactericidal activity. Finally, we demonstrate that verapamil increases efficacy of bedaquiline and delamanid antibiotic therapy. Taken together, our findings suggest that studying virulent clinical strains in an advanced cell culture system is a powerful adjunct to established methodologies to evaluate new interventions for TB.

1. Introduction

Tuberculosis (TB) continues to be a global epidemic, killing approximately 1.5 million people annually, and unfortunately, the COVID-19 pandemic is likely to significantly worsen TB control [1]. Furthermore, *Mycobacterium tuberculosis* (Mtb), the causative bacterium, is becoming progressively more resistant to antibiotics [2]. Standard treatment takes a minimum of 6 months, and MDR-TB patients often require longer treatment for 18 months, with extensive drug side effects [3]. Consequently, there is a pressing need for shortening therapy and discovering new chemotherapeutics [4].

Mtb H37Rv is a standard laboratory reference strain, which is very widely used for experimental purposes around the world. However, it was last isolated from a patient in 1905 [5, 6] and has been repeatedly subcultured in broth culture since then. Consequently, H37Rv has been widely proposed to be attenuated compared to clinical strains [7, 8]. Modern circulating Mtb strains have been classified into multiple lineages [9], and some, such as lineage 2 Beijing isolates, have contributed to large outbreaks of TB globally [10, 11].

Standard TB treatment involves four antibiotics initially, rifampicin, isoniazid, pyrazinamide, and ethambutol, for two months, followed by rifampicin and isoniazid for four months. Treatment of drug-resistant Mtb requires longer courses of antibiotics, typically for greater than 12 months, with second-line agents often having lesser killing efficacy or a worse side effect profile, such as moxifloxacin, D-cycloserine, para-amino salicylic acid, linezolid, and amikacin. The most recently approved agents are bedaquiline and delamanid [3, 12]. Recent studies of shorter treatments have had variable results [13–15], demonstrating that innovative technologies and new methods to investigate mechanisms of novel antibiotics are needed to predict optimal combinations of antimicrobial agents.

Enhanced drug resistance can be due to upregulation of bacterial efflux pumps, either through mutation or increased activity [16–20]. In the zebrafish model of *M. marinum* infection, multidrug tolerance develops in replicating mycobacteria by a macrophage-induced efflux mechanism [21]. Importantly, intramacrophage residence of the bacteria contributed to the phenomenon. Efflux pump inhibitors such as verapamil reduced tolerance to antibiotics including isoniazid and rifampicin [22], and MDR strains developed macrophage-induced drug tolerance and utilized efflux pumps for intracellular growth. Consequently, the calcium channel blocker verapamil has emerged as a potential adjunctive chemotherapy for TB [23–25].

In this study, we investigate pathogenicity and antibiotic sensitivity of Mtb H37Rv compared to clinical Mtb isolates in broth culture and a 3-D primary human cellular granuloma model of TB infection, where host gene expression reflects events in patients more closely than standard cell culture [26–28], and Mtb is pyrazinamide sensitive [29]. We demonstrate significant differences between laboratory and clinical strains in the 3-D system. We then investigate MDR-TB and emerging therapies and combination treatment, further demonstrating the potential of adjunctive verapamil to increase antibiotic efficacy against clinical isolates when tested in an advanced cell culture model.

2. Experimental Procedures

2.1. Mycobacteria Culturing and Reagents. The reference strain *Mycobacterium tuberculosis* H37Rv originated from Prof. Friedland's laboratory (Imperial College London), originally from the Pasteur Institute, and Erdman and CDC 1551 strains were a gift from Dr Rawkins at Public Health England, Porton Down, UK. We obtained drug-sensitive clinical isolates and MDR-TB from Prof. Drobniewski (Imperial College London) [11]. Bioluminescent bacteria were routinely cultured in Middlebrook 7H9 medium (BD Biosciences, Oxford) supplemented with 10% ADC enrichment (SLS), 0.2% glycerol, and 0.02% Tween 80 with kanamycin (25 μg/ml) at 37°C in an incubator with shaking at 200 rpm. The 2-year-old culture of the Beijing strain, 0414B lux, was generated by continuously repeating weekly 200 μl subculture into a freshly prepared 2 ml broth for this period. Bacteria were cultured until optical density of 0.6 was reached, which is equivalent to about 1×10^8 CFU/ml. Either spectrophotometer (WPA Biowave CO8000 cell density meter, UK) or luminometer (GloMax® 20/20 Single Tube Luminometer; Promega, UK; detecting luminescence) was used to observe mycobacterial proliferation in 7H9 media. Reagents in this study were mainly Sigma-Aldrich acquired apart from delamanid and bedaquiline, which were bought from Adooq Bioscience, and tariquidar, diltiazem, amlodipine, and carbonyl cyanide m-chlorophenyl hydrazone (CCCP), which were obtained from Tocris.

2.2. Generating Bioluminescent Mycobacteria by Electroporation. Bioluminescent mycobacteria were generated by electroporation of pMV306hsp+LuxG13 plasmid (Addgene # 26161), into *M. tuberculosis* H37Rv, Erdman, CDC1551, clinical isolates, and MDR strains (Table S1) as previously described [30, 31]. We used 7H11 agar plates with kanamycin (25 μg/ml) to select the strains transformed with an integrating vector. Luminescence of five randomly picked colonies was recorded, and the transformants were checked by PCR with oligonucleotides (forward: 5′-AACCGTATTAC CGCCTTTGA-3′ and reverse: 5′-TATCAGCCCGTACC AGCATT-3′) amplifying the corresponding promoter and reporter gene.

2.3. Infection of Human Peripheral Blood Mononuclear Cells. Ethical approval was provided by the National Research Ethics Service Committee South Central-Southampton A, ref. 13/SC/0043. The National Health Service Blood and Transplant, Southampton, UK, supplied us with single-donor buffy coats, from which peripheral blood mononuclear cells (PBMCs) were isolated using density gradient centrifugation over Ficoll-Paque (GE Healthcare Life Sciences, UK). Host cells were then infected with luminescent mycobacteria at a multiplicity of infection (MOI) of 0.1. After overnight incubation at 37°C in 5% CO_2, the infected PBMCs were treated with Versene solution for 10 min and neutralised by HBSS without Ca/Mg (Gibco). The cells were detached by scraping, placed in 50 ml falcon tubes, topped up with HBSS, and spun at $320 \times g$ for 8 min at 4°C. The supernatant was then decanted, and the remaining pellet was resuspended in RPMI 1640 solution with added 10 μg/ml of ampicillin, 2 mM of glutamine, 25 μg/ml of kanamycin, and 10% of human AB serum (to form a complete RPMI medium).

2.4. Cell Encapsulation to Form 3-D Culture Microspheres. Microspheres were generated as previously described [26, 29, 32]. In short, to obtain a 3-D culture, we resuspended Mtb-infected host cells in complete RPMI medium and combined with alginate-collagen matrix at 1×10^6 cells per ml. Microspheres were obtained by introducing the sterile mix into the electrostatic bead generator (Nisco, Zurich, Switzerland) as described previously [33]. Next, we equally distributed microspheres into 2 ml Eppendorfs, immersed them in 1 ml of complete RPMI medium, and kept at 37°C with 5% CO_2. Bacterial bioluminescence was observed with a GloMax® 20/20 Luminometer. In order to carry out colony counts, Mtb was released from microspheres by dissolving in 55 mM sodium citrate/10 mM EDTA with 1% saponin in

HBSS, pelleting at 10,000 × g in a Heraeus™ Pico™ microcentrifuge, and plating onto 7H11 agar. Colony-forming units were counted at three weeks.

2.5. Imaging by Microfocus X-Ray Computed Tomography (μCT). μCT imaging was performed on the Nikon Med-X micro-CT scanner, optimised for biomedically relevant low-contrast specimens. The equipment is supplied with a 130 kVp X-ray source and a 2 × 2 k flat panel detector allowing to obtain images at ~3 μm spatial resolution. Microspheres containing PBMCs infected with Mtb H37Rv were harvested at day 14 and prepared for imaging. Samples were fixed for 1 h at room temperature and then overnight at 4°C in 3% glutaraldehyde in 0.1 M cacodylate buffer (pH: 7.4) with an osmolarity of 850 mOsm plus 2 mM $CaCl_2$. Fixed samples were then washed with the 0.1 M cacodylate buffer (pH: 7.4) and postfixed with 2% osmium tetroxide in 0.1 M cacodylate buffer (plus 2 mM $CaCl_2$ and 2.3 M sucrose). A sample was, then, treated with a single wash step using a distilled water prior to staining it with 2% uranyl acetate (aq). Samples were dehydrated through a series of ethanol submersion steps in 30%, 50%, 70%, 95%, and 100% alcohol solutions. The final 100% ethanol step was carried out twice. Next, the samples were immersed in acetonitrile in order to facilitate the passage from ethanol to resin. Samples were kept overnight in a 50 : 50 acetonitrile/TAAB resin mixture. In the next day, a fresh resin was prepared and samples were incubated in it for further 6 h. Subsequently, the samples were moved to embedding capsules with fresh TAAB resin. This resin block was scanned with μCT. The 3-D stack generated had a voxel size of 2.7 μm.

2.6. 3-D Image Processing. On a specific Amira workstation, 3-D image segmentation and analysis were done using FEI Amira software (version 6.4.0). In addition to the Wacom Cintiq 22HD touchscreen monitor (resolution 1920 × 1080 pixels), the workstations include an Intel Xeon processor with 24 cores, 192 GB of RAM, and an Nvidia Quadro K4200 4 GB graphic card. Manual segmentation of microspheres containing aggregates (red), PBMC aggregates (blue), and single PBMCs (yellow) was carried out on the 3-D dataset of the resin block containing microspheres. 3-D reconstruction of the highlighted areas occurred using the "Generate Surface" feature of Amira software. A smoothing function was applied to all three different labels to reduce the staircase effect. To visualise the result as a 3-D representation of the manual segmentation, the "Surface View" object was attached to the surface file.

2.7. Scanning Electron Microscopy (SEM). Initial fixation and processing to the completion of ethanol drying was as above. The microspheres were inserted in a metal holder with a grid after the final step of ethanol. Prior to SEM imaging, the lid of the holder was shut and the entire holder put in an absolute ethanol-filled glass vial. In order to achieve critical point drying, the samples were dried with a Balzers CPD 030 drier. On a stub covered with two-sided tape, dried microspheres were sprayed with gold and palladium (Pd), two nonoxidising metals, utilizing the Polaron E5100 sputter coater. This study was conducted with a FEI Quanta 200 scanning electron microscope for the acquisition of SEM images. Up to 30 kV of power and 100,000x magnification are available with this system. Ten kilovolts of power was used for acquisitions.

2.8. Eukaryotic Cell Viability/Toxicity Assays. Microspheres were equally distributed into two 96-well plates and incubated at 37°C. At days 3 and 7, respectively, one plate was sacrificed for cell viability analysis. Promega's CellTiter-Glo 3-D cell viability assay was performed following the manufacturer's specifications. Cellular necrosis in microspheres was measured using CytoTox-Glo cytotoxicity assay (Promega). The GloMax® Discover 96-well plate reader (Promega, UK) was used to monitor the luminescence. Additionally, cell toxicity was determined by measuring the release of lactate dehydrogenase (LDH) with a colorimetric activity assay (Roche, Burgess Hill, United Kingdom). The collected supernatants were stored at 4°C for up to 7 days prior to analysis.

2.9. Luminex Analysis. Supernatants were collected at day 3 and store at -20°C. Samples were sterilized by filtration through a 0.22 mM Durapore membrane (Millipore) [34]. We followed the manufacturer's protocol to determine concentrations of cytokines (Life Technologies, UK) and MMPs (R&D Systems, UK) in the samples using a BioPlex 200 platform (Bio-Rad, Hemel Hempstead, United Kingdom). Cytokine concentrations were measured using the cytokine 35-plex human panel (Thermo Fisher Scientific, UK). Analyses of MMP concentrations were done by MMP fluorokine multianalyte profiling (R&D Systems, Abingdon, UK).

2.10. Statistical Analysis. All experiments were carried out on a minimum of two separate occasions from different donors as biological replicates and each time with a minimum of three technical replicates. GraphPad Prism was utilized to carry out statistical analyses. Either ordinary one-way or 2-way ANOVA Tukey's multiple comparison tests were used to compare groups.

3. Results

3.1. Differential Growth of Mtb Strains in Middlebrook 7H9 Broth versus 3-D Microspheres. To study Mtb proliferation in the context of host cells and extracellular matrix, we generated 3-dimensional microspheres, which consisted of human primary peripheral blood mononuclear cells, Mtb, and collagen (type I) using bioelectrospray methodology as previously described [26, 27, 29, 32, 35]. Scanning electron microscopy demonstrated the external symmetry of the spheres (Figure 1(a)). We characterised cellular aggregation within spheres by microcomputed tomography (μCT), which demonstrated multicellular granuloma formation at day 7 (Figures 1(b) and 1(c) and Supplemental Video 1).

To monitor Mtb growth in our 3-D system, we generated luminescent clinical isolates by incorporating the Lux operon (Table S1) [30]. Microsphere luminescence closely correlates with colony counts, permitting longitudinal analysis of growth within microspheres [29]. First, we compared Mtb

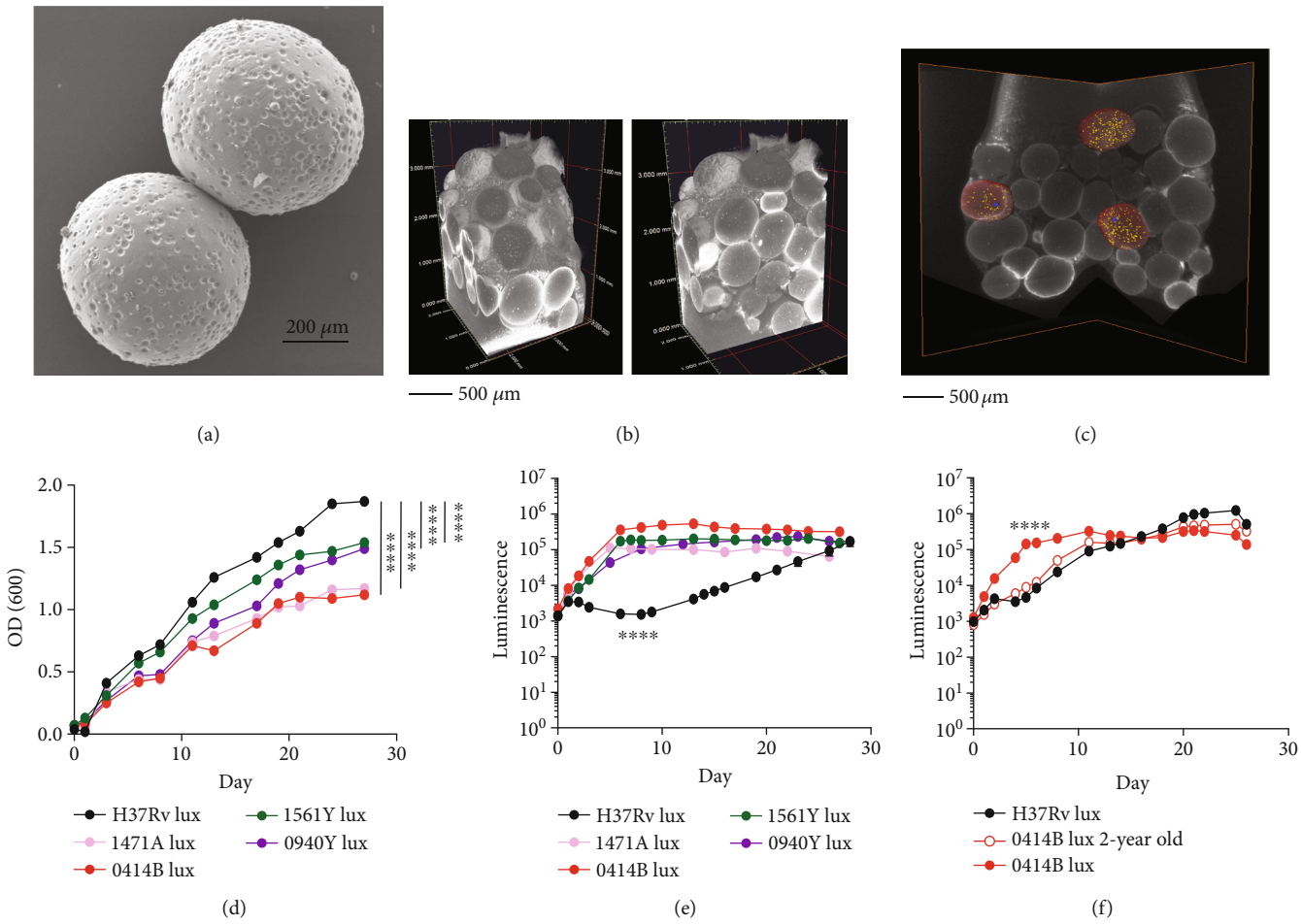

FIGURE 1: Mycobacterial clinical isolates grow more rapidly in the 3-D microsphere model. (a) Scanning electron microscopy of microspheres to demonstrate appearance. (b, c) Micro-CT scan (μCT) of embedded microspheres with 3-D reconstruction. Spheres appear different sizes as different levels have been captured within the block. (b) External appearance and cut surface. (c) Sagittal section. Representative microspheres were marked in red, showing equal distribution of PBMCs within microsphere (yellow). A cellular aggregate is visible in the centre sphere (blue). (d) H37Rv lux grows faster than clinical isolates (1561Y lux, 0414B lux) and MDR-TB strains (1471A lux, 0940Y lux) in Middlebrook 7H9 broth measured by optical density (OD) at 600 nm. Experiments were performed in triplicate. (e) Conversely, H37Rv lux growth in the 3-D system is attenuated in comparison to clinical isolates measured by luminescence. (f) Beijing lineage clinical isolate 0414B lux becomes attenuated after continuous 2-year culturing in broth when studied in the microsphere system, growing at a similar rate to the lab strain H37Rv lux, in contrast to freshly defrosted 0414B lux strain. (e, f) Data are the mean ± SEM of an experiment performed in triplicate and are representative of two separate experiments. (d–f) Statistics: 2-way ANOVA Tukey's multiple comparison test; $^{****}p < 0.0001$.

proliferation in Middlebrook 7H9 broth to growth within microspheres. The standard laboratory strain, H37Rv, grew significantly more rapidly in broth culture than the clinical isolates ($p < 0.0001$) (Figure 1(d)). In contrast, in the 3-D system, H37Rv was significantly attenuated in comparison to clinical isolates, which proliferated much more rapidly over time (Figure 1(e)). A similar pattern was observed when H37Rv was compared with two other reference Mtb strains, CDC1551 and Erdman (Figure S1). We then repeatedly subcultured one of the clinical isolates of Beijing origin, 0414B, continuously in 7H9 broth for two years. This prolonged *in vitro* culture attenuated growth rate in infected host cells in the 3-D model, to a similar extent to H37Rv, relative to freshly defrosted and cultured 0414B (Figure 1(f)). Therefore, the standard laboratory strain, H37Rv, is attenuated compared to clinical isolates when analysed in a 3-D primary human cell culture model.

3.2. Despite Increased Proliferation, the Clinical Strain Is Not Cytotoxic and Cytokine Secretion Is Suppressed. Next, we investigated the effect of increased growth of the clinical isolate 0414B on host cells in the 3-D system relative to the laboratory strain H37Rv. Host cells infected with either Mtb strain survived better relative to uninfected PBMCs at day 3, analysed by two different readouts, likely due to infection upregulation of prosurvival growth factors (Figures 2(a) and 2(b)). However, we did not observe these differences using the CellTiter-Glo 3-D cell viability assay at this time point (Figure 2(c)). Comparing Mtb-infected cells, a significant increase in toxicity with the clinical strain was only observed

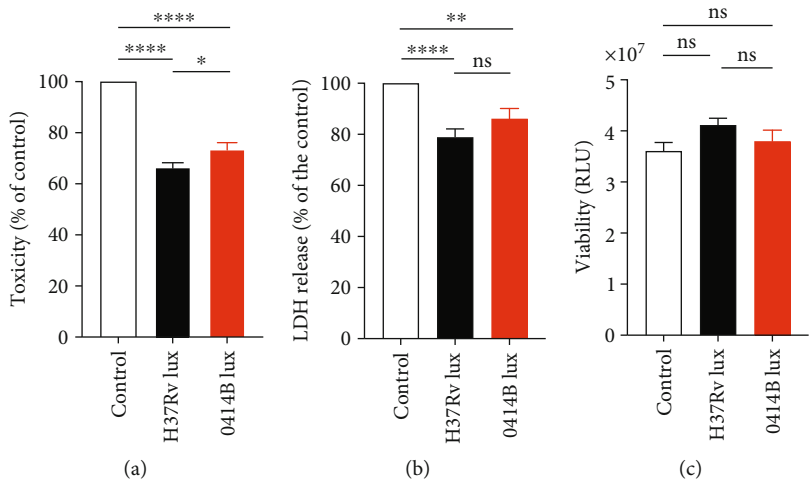

Figure 2: Host cells infected with Mtb H37Rv or a clinical strain have similar survival despite differences in bacterial proliferation. (a, b) After infection with H37Rv lux (black) or 0414B lux (red), cells survived better than uninfected cells. A minimal difference was observed in relative host cell toxicity between strains measured by (a) CytoTox-Glo cytotoxicity assay, but no significant differences were seen with (b) LDH cytotoxicity assay and (c) CellTiter-Glo 3-D cell viability assay between strains at day 3. Data are mean ± SEM of 3 separate experiments. (a–c) Statistics: ordinary one-way ANOVA with Tukey's multiple comparison test; $^{****}p < 0.0001$, $^{**}p < 0.01$, $^{*}p < 0.1$, and $^{ns}p > 0.05$.

using CytoTox-Glo cytotoxicity assay (Figure 2(a)), not with the LDH assay or CellTiter-Glo 3-D cell viability assays at the 3-day time point (Figures 2(b) and 2(c)). There were some differences observed at the 7-day time point, with the clinical strain causing greater toxicity as measured by LDH release (Figure S2B). These differences likely result from the technical features of the assays used, with LDH released from dying cells and stable for 7 days, so this provides a slightly different measure of cell death to the CytoTox-Glo cytotoxicity assay and CellTiter-Glo assay. Later time points did not reveal any significant differences between strains using the two luminescent cell viability assays (Figure S2A and C).

We compared the immunological response elicited by each strain at day 3, profiling secretion of inflammatory mediators by Luminex array. Despite the significantly higher mycobacterial load, secretion of proinflammatory cytokines was reduced from 0414B-infected microspheres in comparison to the lab strain H37Rv (Figure 3). Suppressed cytokine release included TH_1 cytokines, TH_2 cytokines, and some chemokines (Figure 3 and Figure S3). The secretion of other analytes, such as IL-17A, IL-8, and MCP-1, was upregulated by Mtb infection equally in response to both strains, indicating that 0414B did not induce a global hyposecretory state. Similarly, secretion of the proteases matrix-metalloproteinase-1 (MMP-1) and MMP-7 was equally upregulated by H37Rv and 0414B (Figure 3 and Figure S3).

3.3. Clinical Isolates Are Less Susceptible to Antibiotics in the 3-D System. Having observed accelerated growth but reduced cytokine secretion for 0414B relative to H37Rv in the microsphere system, we investigated relative efficacy of antibiotics against each strain. Cell culture media around spheres were supplemented with standard first-line antibiotics, rifampicin, isoniazid, and pyrazinamide, at physiological concentrations (1 g/ml, 0.25 g/ml, and 500 g/ml, respectively), on day 1 [29]. The three-dimensional system demonstrated inhibitory effects of all three antibiotics on H37Rv growth (Figure 4(a)) as previously reported, with luminescence falling progressively to baseline [29]. In contrast, after initial suppression, the clinical isolate 0414B regrew at day 12 despite incubation with rifampicin and isoniazid (Figure 4(d)). Furthermore, pyrazinamide was much less effective against the clinical isolate relative to the laboratory strain, with complete killing of H37Rv compared to temporary retardation of growth of 0414B. We tested a second clinical isolate, 1292F (lineage 4, Ural origin) with the four first-line drugs and once more observed regrowth. Again, pyrazinamide was less effective (Table 1). Therefore, clinical isolates are relatively more resistant to first-line antibiotics in the 3-D model compared to the laboratory strain H37Rv.

With the emergence of drug-resistant TB, novel and repurposed second-line antibiotics have become increasingly important [2]. Therefore, we analysed amikacin, moxifloxacin, D-cycloserine, and linezolid in the microsphere system. Moxifloxacin and linezolid (5 μg/ml and 24 μg/ml, respectively) completely inhibited the growth of all the drug-sensitive strains in the 3-D system (Figures 4(b) and 4(e) and Table 1). Amikacin was also as effective (Figures 4(b) and 4(e) and Table 1), except for the Ural strain, 1292F, where the bacterial killing was relatively reduced (Table 1). D-Cycloserine was effective against H37Rv but minimally effective for the 0414B strain (Figure 4(e)) but was efficacious against 1561Y and had intermediate activity against 1292F (Table 1). PAS (20 μg/ml) had similar efficacy against all clinical isolates examined, partially inhibiting growth (Table 1).

Finally, we tested emerging antibiotics bedaquiline and pretomanid (PA-824). Bedaquiline effectively killed the laboratory strain H37Rv but was significantly less efficacious

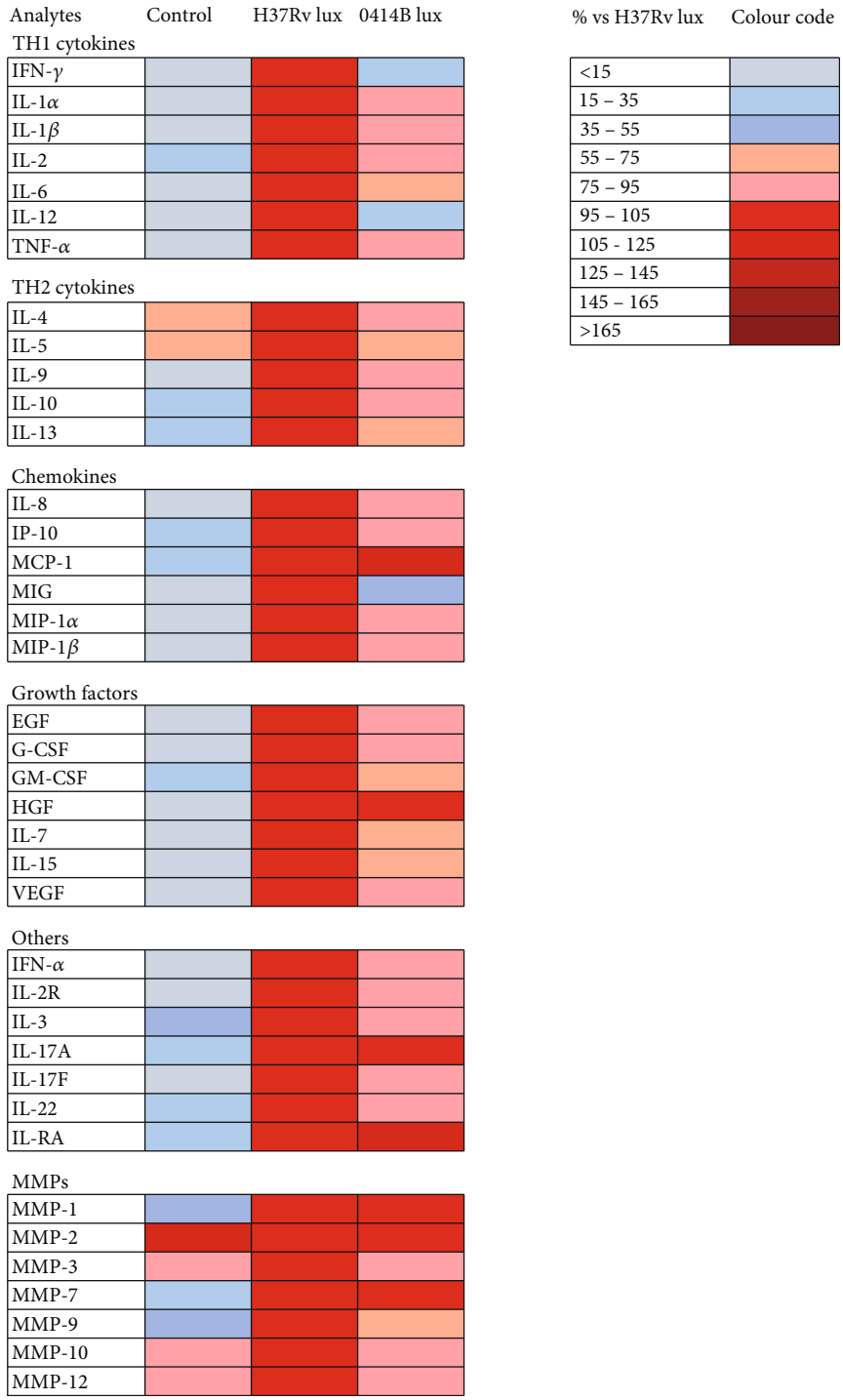

Figure 3: The clinical Mtb strain is less proinflammatory than 0414B. A heatmap of differences in cytokine secretion by PBMCs within microspheres after infection either with the laboratory strain H37Rv lux or the clinical isolate 0414B lux, measured at day 3 by Luminex array. Cytokine secretion was normalised to concentration of H37Rv-infected cells (data are presented as a percentage normalised to H37Rv lux strain). Secretion of thirteen analytes was significantly reduced for the clinical strain in contrast to the lab strain, despite greater bacterial proliferation. Other analytes, such as IL-17A, MCP-1, MMP-1, and MMP-7, were equally upregulated by Mtb infection. Control: uninfected PBMCs within microspheres. Normalised data from two donors analysed in triplicate are presented.

against the 0414B strain even at 10 μg/ml (Figures 4(c) and 4(f)). PA-824 completely inhibited growth of all strains studied (Figures 4(c) and 4(f) and Table 1). These studies further confirmed increased antibiotic resistance in clinical strains relative to H37Rv.

3.4. Effect of Anti-TB Drugs on MDR-TB Growth in 3-D Model. Next, we investigated the efficacy of these antibiotics against MDR-TB in the 3-D model. As a proof of principle, we selected two MDR-TB clinical isolates 1471A and 0940Y, both belonging to the Beijing sublineage (Table S1), which

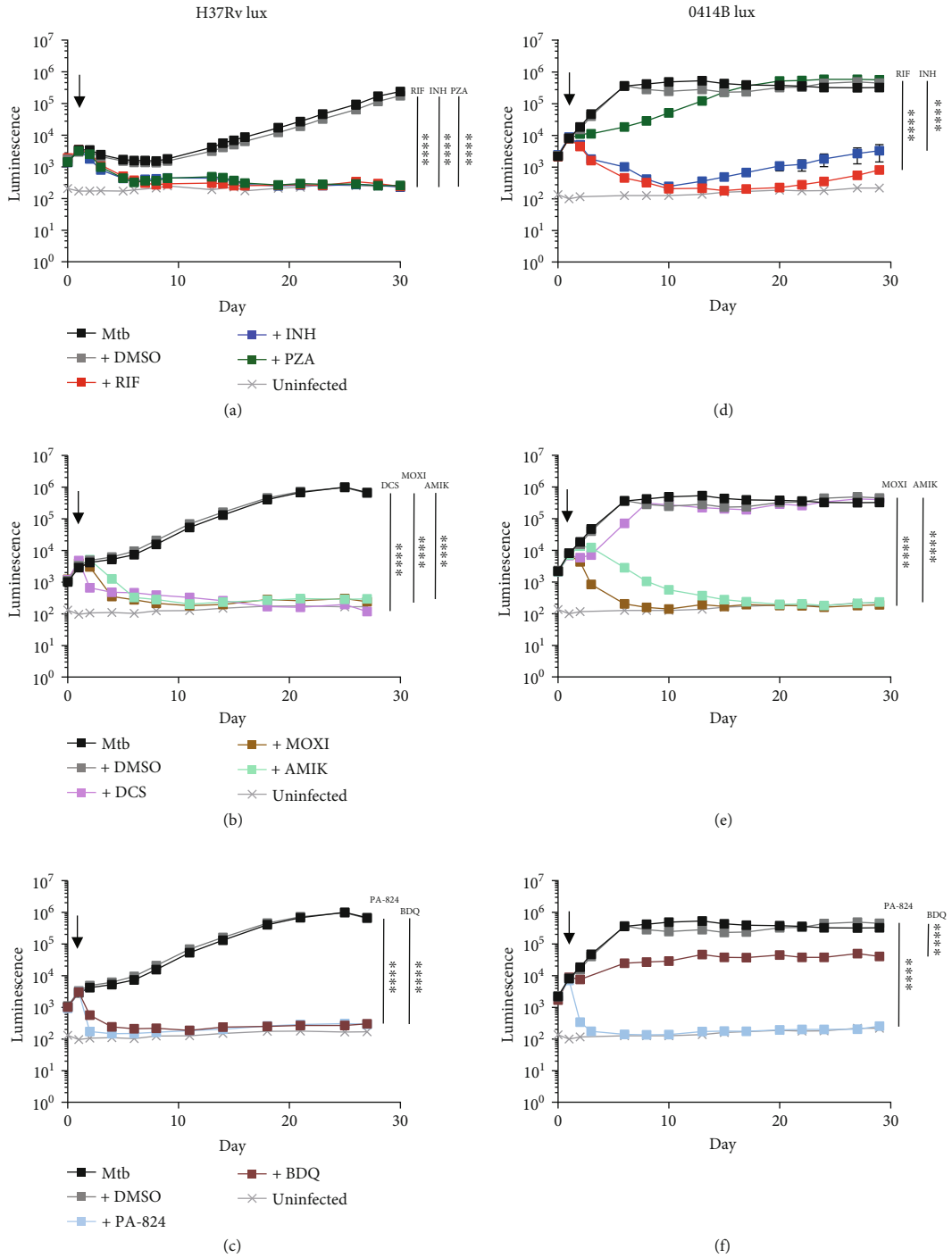

Figure 4: The 0414B clinical strain is antibiotic resistant relative to Mtb H37Rv. Antibiotics were added at day 1 to the 3-D system and Mtb growth measured with luminescence. Standard drugs: rifampicin (RIF, 1 μg/ml, dark red), isoniazid (INH, 0.25 μg/ml, navy blue), and pyrazinamide (PZA, 500 μg/ml, dark green). Second-line drugs: amikacin (AMIK, 15 μg/ml, mint green), moxifloxacin (MOXI, 5 μg/ml, light brown), and D-cycloserine (DCS, 20 μg/ml, lilac). Emerging drugs: bedaquiline (BDQ, 10 μg/ml, dark brown) and pretomanid (PA-824, 3 μg/ml, light blue). H37Rv lux growth was inhibited by all antibiotics tested (a–c). The clinical isolate 0414B regrew at day 12 despite incubation with RIF and INH, and PZA was much less effective against the clinical isolate relative to the laboratory strain (d). From the second-line antibiotics, amikacin and moxifloxacin completely inhibited the clinical isolate's growth, but D-cycloserine had only a minor effect (e). Similarly, bedaquiline had only a partial effect in contrast to PA-824, which was very effective against 0414B lux (f). Dimethyl sulfoxide (DMSO) used as solvent for rifampicin, bedaquiline, and pretomanid in the control sample did not affect the growth of Mtb. Background level of luminescence is designated by crosses (x). Black arrow specifies antibiotic addition. The experiment was performed in triplicate on two separate donors, and a representative experiment is shown. Statistical analyses were done using 2-way ANOVA Tukey's multiple comparison test; $^{****}p < 0.0001$. The data are very consistent, so SEM bars are very narrow and obscured.

Table 1: Summary of the efficacy of antibiotics against different clinical isolates in the 3-D model.

Strain Abx (μg/ml)	RIF 1	INH 0.25	PZA 500	EMB 4	AMIK 15	MOXI 5	DCS 20	LNZ 24	BDQ 10	PAS 20	PA-824 3
Lab											
H37Rv lux	+	+	+	+	+	+	+	+	+	+/-	+
Sensitive											
1292F lux	+	+	+/-	+	+/-	+	-/+	+	+	+/-	+
1561Y lux	+	+	+/-	+	+	+	+	+	+/-	+/-	+
0414B lux	+	+	-/+	+	+	+	—	+	-/+	+/-	+
MDR											
1471A lux	—	—	-/+	—	+	+	—	+	—	+/-	+
0940Y lux	—	—	—	—	+	+	—	+	-/+	+/-	+

RIF: rifampicin; INH: isoniazid; PZA: pyrazinamide; EMB: ethambutol; AMIK: amikacin; MOXI: moxifloxacin; DCS: D-cycloserine; LNZ: linezolid; BDQ: bedaquiline; PAS: para-aminosalicylic acid; PA-824: pretomanid.

have previously been characterised phenotypically by standard assays and genotypically [11]. Strain 1471A was resistant to rifampicin, isoniazid, and ethambutol, and strain 0940Y was resistant to rifampicin, isoniazid, and pyrazinamide based on standard individually validated liquid culture methodology. As expected, rifampicin, isoniazid, and ethambutol had no effect on 1471A growth, and pyrazinamide had a moderate inhibitory effect (Figure 5(a)). Again, the pyrazinamide efficacy was reduced relative to H37Rv in the 3-D model. Strain 0940Y was resistant to rifampicin, isoniazid, and pyrazinamide, as anticipated. Unexpectedly, the strain also was resistant to ethambutol in our system (Figure 5(d)). Ethambutol is a bacteriostatic agent at the concentrations used, and this may reflect the difficulty of reliable microbiological assays for this drug.

From the second-line drugs investigated, only D-cycloserine at the lower concentration of 20 μg/ml had no efficacy against the two strains in the 3-D system (Figures 5(b) and 5(e)). Amikacin, moxifloxacin, and linezolid completely inhibited bacterial growth of both strains (Figures 5(b), 5(c), 5(e), and 5(f) and Table 1). PAS and PA-824 were similarly effective in bacterial killing against the laboratory strain H37Rv and for both MDR strains (Figures 5(c) and 5(f) and Table 1). Bedaquiline (10 μg/ml) had no effect inhibiting 1471A growth, while it moderately inhibited 0940Y growth (Figures 5(c) and 5(f)).

3.5. Verapamil Potentiates the Effect of Emerging Antibiotics in the 3-D System. These data demonstrate inherent antibiotic resistance in all Mtb clinical strains relative to H37Rv and confirm further additional resistance within the MDR strains, suggesting that efflux pumps may be contributing to resistance and highlighting the need to investigate adjunctive therapy to increase bactericidal activity [25]. We focused on bedaquiline and delamanid, important new MDR-TB drugs approved and recommended for treatment [2]. Delamanid is relatively understudied with a partially defined mechanism of action [36]. In 7H9 broth, regrowth occurred after initial killing even at a relatively high concentrations of delamanid (10 μg/ml) (Figures 6(a) and 6(b)). In contrast, delamanid fully inhibited bacterial growth in the 3-D system (Figures 6(c) and 6(d)), demonstrating greater efficacy in the microsphere system relative to standard broth. The high delamanid concentrations required suggested that efflux pump activity contributed to antibiotic resistance, and so, we investigated this further.

Verapamil, a Ca^{2+} channel blocker, potentiates the killing of mycobacteria with rifampicin, isoniazid [22–24], or bedaquiline [21, 37, 38]. Consistent with these observations, we demonstrated that verapamil potentiated the effect of bedaquiline in the 3-D system in killing both laboratory and clinical strains (Figures 7(a) and 7(d)). The effect was most marked for the clinical strain, changing a minor suppression of growth to rapid killing, and a similar effect was observed in 7H9 broth (Figure S4A, B). Next, we investigated whether verapamil could also potentiate the effect of delamanid. Delamanid efficacy was augmented by verapamil in the 3-D system for the clinical isolate 0414B, preventing regrowth at late time points (Figures 7(b), 7(c), 7(e), and 7(f)). In 7H9 broth, regrowth of both strains was delayed in the presence of verapamil together with delamanid, and this effect was greater for the clinical isolates (Figure S4B, C, E, F).

Finally, we investigated whether other Ca^{2+} channel blockers and efflux pump inhibitors had a similar potentiating effect on delamanid as verapamil (Figure S5A). In a host environment, verapamil is an inhibitor of broad-spectrum ABC transporter systems (e.g., P-glycoprotein (P-gp/ABCB1) also known as multidrug resistance protein 1 (MDR1)), and so, we studied a P-gp-specific, third-generation inhibitor, tariquidar, which is also known to inhibit breast cancer resistance protein (BCRP/ABCG2) [39]. Tariquidar did not potentiate the effect of delamanid (0.5 μg/ml) at concentrations ranging 0.5-50 μg/ml (Figure S5B). Similarly, diltiazem, a nondihydropyridine (DHP) member of the calcium channel blocker class, had no effect (Figure S5C), while amlodipine, which is a dihydropyridine (DHP) calcium channel blocker, had very minor potentiating effect on delamanid at 30 μg/ml (Figure S5D). Additionally, we investigated two compounds that act not only at the host level but also directly on mycobacteria. Chlorpromazine, a

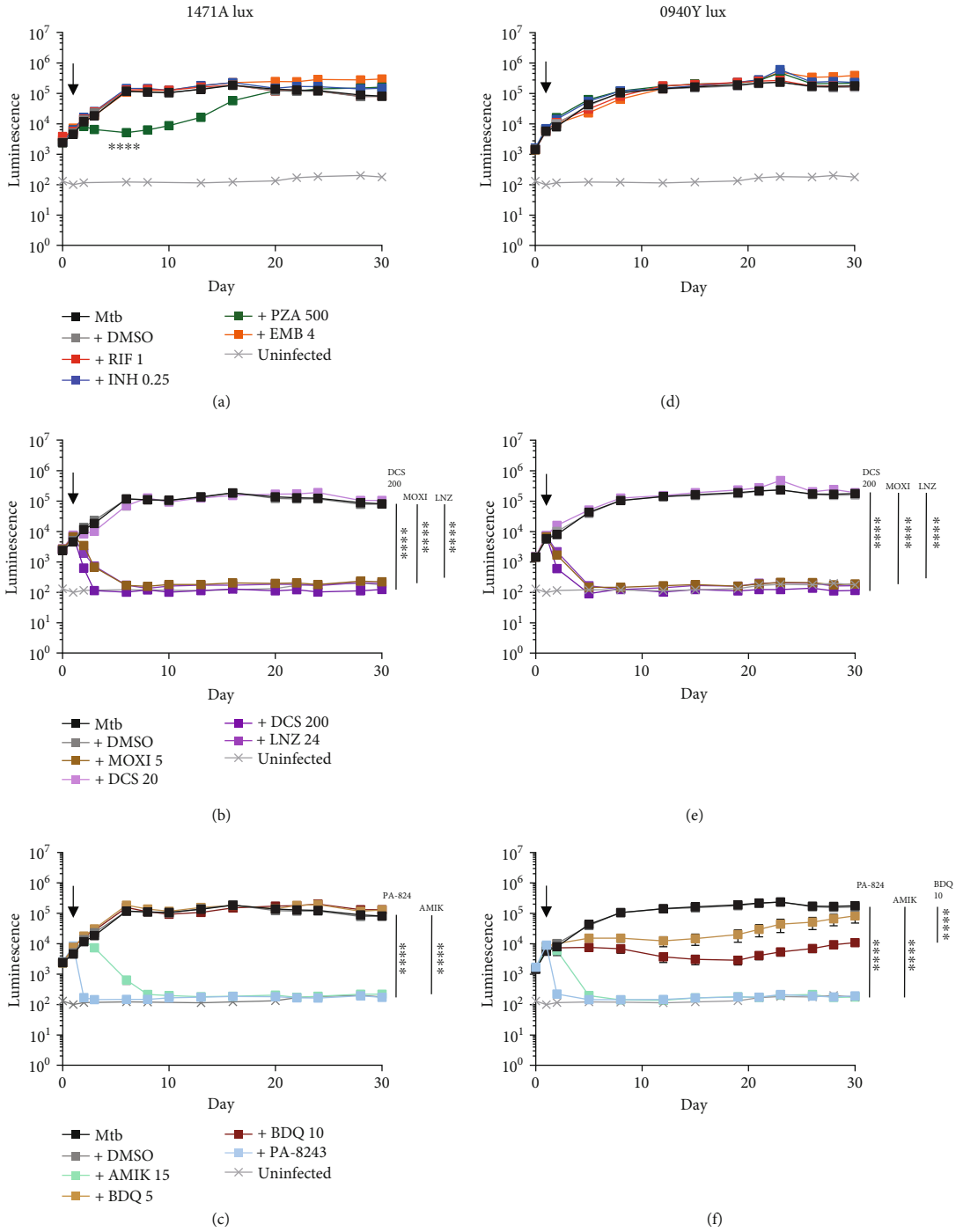

Figure 5: Multi-drug-resistant (MDR) strains demonstrate extensive antibiotic resistance. Antibiotics were added at day 1 to the 3-D model and Mtb growth measured with luminescence. First-line drugs: rifampicin at 1 μg/ml (RIF 1, dark red), isoniazid at 0.25 μg/ml (INH 0.25, navy blue), pyrazinamide at 500 μg/ml (PZA 500, dark green), and ethambutol at 4 μg/ml (EMB 4, orange). Second-line drugs: moxifloxacin at 5 μg/ml (MOXI 5, light brown), D-cycloserine at 20 μg/ml (DCS 20, lilac) and 200 μg/ml (DCS 200, dark purple), and linezolid at 24 μg/ml (LNZ 24, midpurple). Emerging drugs: bedaquiline at 5 μg/ml (BDQ 5, beige) and 10 μg/ml (BDQ 10, dark brown) and pretomanid at 3 μg/ml (PA-824 3, light blue). (a) 1471A lux strain confirmed resistance to rifampicin, isoniazid, and ethambutol and showed partial sensitivity to pyrazinamide. (b, c) Growth of this multi-drug-resistant clinical isolate was unaffected by the lower concentration of D-cycloserine and bedaquiline (both concentrations tested). 0940Y lux strain was resistant to all (d) first-line antibiotics and (e) D-cycloserine at the lower concentration. (f) 0940Y had partial sensitivity to bedaquiline. Bacteria were fully inhibited by all other antibiotics examined. Mtb growth was unaltered by adding DMSO, used as solvent for rifampicin, linezolid, bedaquiline, and PA-824. Crosses (x) designate background level of luminescence. Black arrow shows antibiotic addition. The experiment was performed in triplicate on two separate donors, and a representative experiment is shown. Statistical analyses were carried out using 2-way ANOVA with Tukey's multiple comparison test; $^{****}p < 0.0001$.

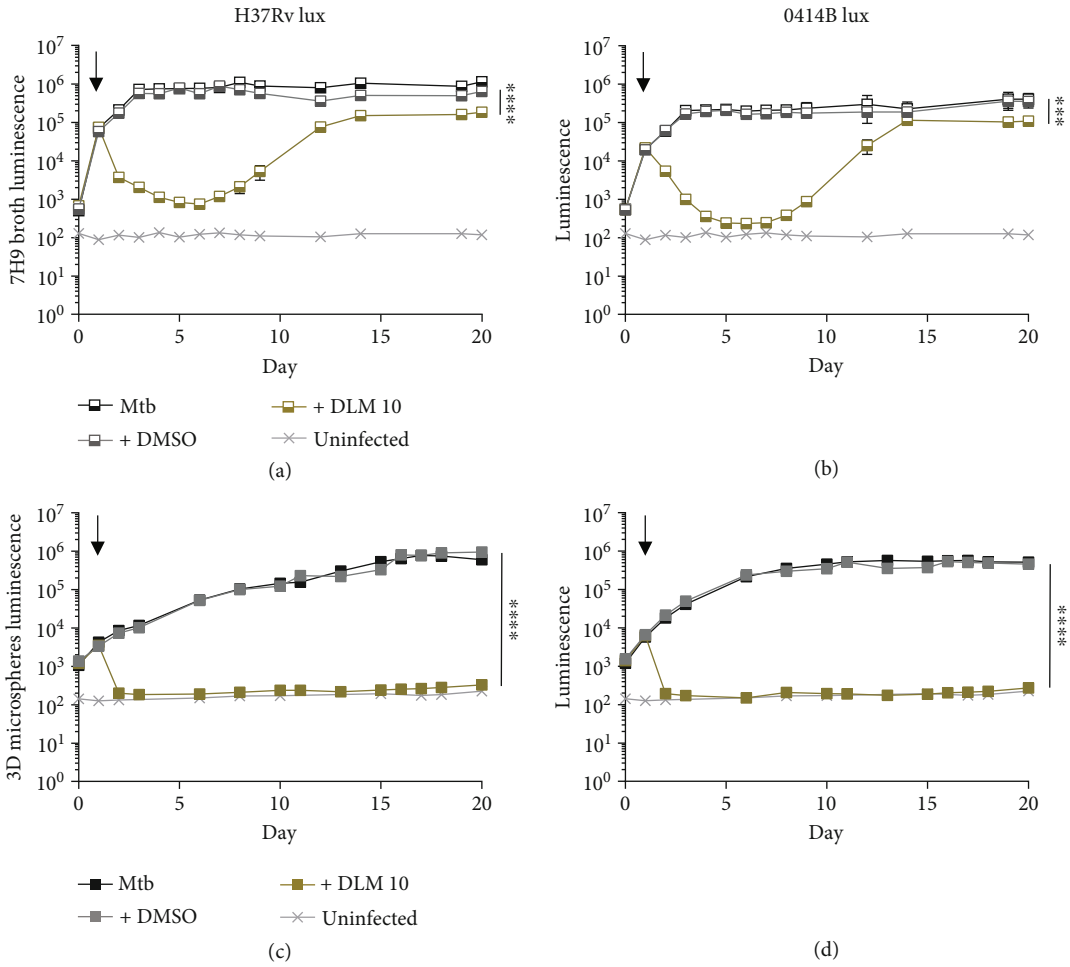

Figure 6: Delamanid is more effective in microspheres than 7H9 broth. Delamanid was added at day 1 to either (a, b) 7H9 broth or (c, d) infected microspheres and Mtb growth monitored by luminescence. (c, d) Bacteria were inhibited to the background level with delamanid at 10 μg/ml (DLM 10, khaki green) in the microsphere system. (a, b) Conversely, delamanid in 7H9 broth was much less effective in killing either H37Rv or O414B. Mtb growth was unaffected by DMSO, used as solvent for delamanid. Background level of luminescence is shown by crosses (x). Addition of antibiotics is marked by a black arrow. The experiment was performed in triplicate on two separate donors, and a representative experiment is shown. Statistical analyses were performed using 2-way ANOVA with Tukey's multiple comparisons test; $^{****}p < 0.0001$ and $^{***}p < 0.001$.

type II NADH dehydrogenase (NDH-2) inhibitor [40] affecting Mtb oxidative phosphorylation, had only minimal potentiating effect, and carbonyl cyanide m-chlorophenyl hydrazine (CCCP), a proton uncoupler [41, 42], had no potentiating effect at the concentrations tested (Figure S5E, F). Overall, none of the compounds investigated exhibited a potentiating effect on delamanid that was as potent at that of verapamil, suggesting that verapamil has a unique mode of action in increasing antibiotic efficacy in relation to bacteria interacting with cells of a host.

4. Discussion

Tuberculosis remains a depressingly persistent global pandemic, and drug resistance is an increasing problem [2]. Consequently, novel systems to evaluate antibiotic agents are needed to identify alternative treatment approaches and combinations. Previously, the typical route of identifying novel antibiotics was through the "three M's" route: minimal inhibitory concentration (MIC), mouse and man [43], centred on enriched liquid culture media for MIC and then minimum bactericidal activity (MBC) determination. Other more complex assays are less frequently employed to identify lead compounds. Although the "3M" approach is simple and straightforward, it does not incorporate the different physiological and anatomical microenvironments of granulomas and cavities in a patient's lung [44, 45] and the effect of these on drug penetration and activity. Consequently, this approach limits selection to compounds that are most effective against rapidly replicating bacteria, potentially omitting antibiotics that work against slowly replicating/dormant Mtb or are only efficacious in the context of a combined drug-host immune response. However, the more complex the assays, the more difficult, costly, and lower the throughput for testing new compounds. In considering the cost of clinical trials, there is significant scope to increase the initial

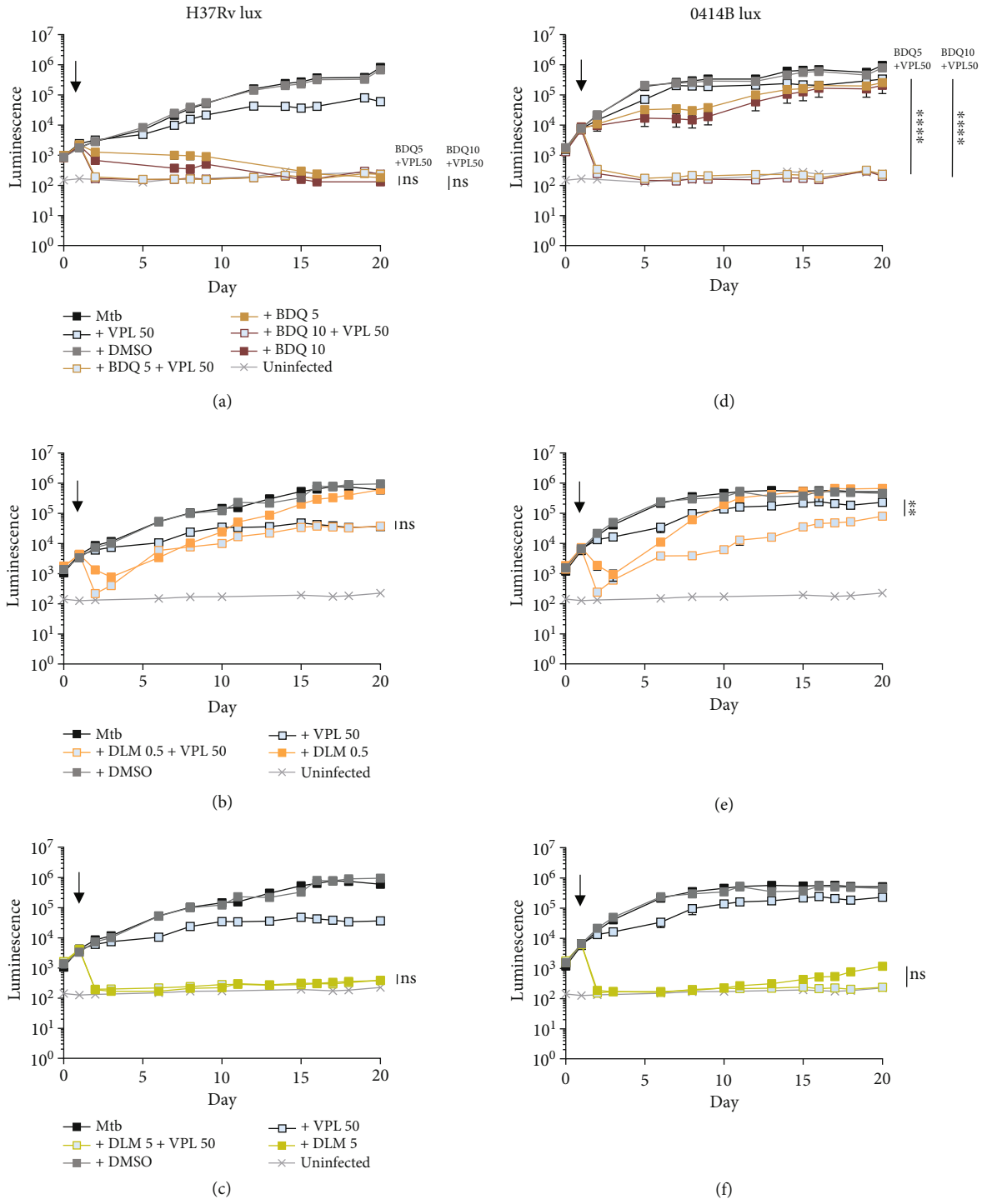

Figure 7: Verapamil increases efficacy of bedaquiline and delamanid in 3-D culture. Compounds were supplied at day 1 to the 3-D system and Mtb growth observed by luminescence: bedaquiline at 5 μg/ml (BDQ 5, beige) and 10 μg/ml (BDQ 10, dark brown), verapamil at 50 μg/ml (VPL 50, light blue), and delamanid at 0.5 μg/ml (DLM 0.5, orange) and 5 μg/ml (DLM 5, light green). Verapamil alone slightly reduced the growth of Mtb in all conditions. Verapamil potentiated the effect of bedaquiline for both H37Rv lux and 0414B lux in the 3-D system (a, d). Delamanid at 0.5 μg/ml combined with verapamil had a greater killing effect on the clinical isolate than on H37Rv (b, e). Delamanid at the higher concentration inhibited the bacterial growth to the background level (c, f). Slight regrowth was observed at a later time point for 0414B lux, which was inhibited when combined with verapamil. Mtb growth was unaffected by DMSO, used as solvent for all the compounds tested. Crosses (x) show background level of luminescence. Black arrow points to antibiotic addition. The experiment was performed in triplicate on two separate donors, and a representative experiment is shown. Statistics: 2-way ANOVA Tukey's multiple comparison test; $^{****}p < 0.0001$, $^{**}p < 0.01$, and $^{ns}p > 0.05$.

screening costs to save future expense; for example, a phase 3 novel antibiotic studies for hospital-acquired bacterial pneumonia cost $89,600 per patient enrolled [46].

Consequently, better *in vitro* systems are required for TB drug discovery [47, 48]. This problem is illustrated by pyrazinamide, which would not have been identified through a traditional strategy; PZA is not bactericidal under standard culture conditions and works optimally under hypoxic conditions at pH 5.5 [49]. Likewise, linezolid is bacteriostatic in standard culture media, but a potent agent as part of combination treatment for M/XDR-TB [2]. The community is moving towards the concept of evaluating new combinations rather than evaluation of single agent. The results of the STREAM 1 trial support this, demonstrating that a short regimen (9-11 months) was noninferior to a long regimen with respect to the primary efficacy outcome and has a similar safety profile [15]. We need to evaluate novel drugs and drug combinations, using different early stage models that can identify agents that complement each other in their ability to penetrate the range of TB lesions and to kill all bacterial subpopulations inside them [43]. In addition, the bacterial strains evaluated need to be standardised for reproducibility and include clinically relevant ones.

Mtb H37Rv has been a mainstay in TB research but was isolated from a patient in the beginning of 20th century and has been repeatedly subcultured since [50, 51]. Here, our 3-D granuloma model shows that relative to the standard laboratory H37Rv strain, the clinical strain 0414B is more virulent, hypoinflammatory, and inherently antibiotic resistant. The coadministration of verapamil increases the efficacy of bedaquiline and delamanid, and this effect is most pronounced for clinical strains. Our findings further highlight the importance of including diverse strains in drug discovery studies [7, 8, 51, 52], while supporting the utility of advanced cell culture models incorporating human cells to refine the drug discovery pipeline [47, 53].

Mtb strains H37Rv and 0414B belong to Mtb lineages 4 and 2, respectively. In Middlebrook 7H9 broth, H37Rv grew much better than other strains investigated belonging to lineage 2 ("modern" Beijing strains) and lineage 4 (reference strains: Erdman and CDC1551), which has been observed previously [54], but conversely was significantly attenuated in the microsphere system compared to these strains. In experiments with mice, lineage 2 strains produced high levels of bacilli in their lungs [55]. Furthermore, studies using 2-D human cell culture systems demonstrated that mycobacteria of this genotype replicate more rapidly in comparison to the laboratory reference strains [56–58] and that lineage 2 strains spread more rapidly between cells than H37Rv [59], supporting our observation of increased pathogenicity.

Increased proliferation of the clinical strain was not associated with greater host cytotoxicity, suggesting Mtb accumulates within host cells without destroying them. H37Rv was hyperinflammatory in contrast to the clinical isolates, inducing less cytokine secretion. Diverse human and animal evidence suggests that the enhanced virulence of the Beijing strains is partially due to induction of lower levels of Th1 cytokines such as TNF-α, IL-6, IL-10, IL-12, and IFN-γ [54, 57, 60–65]. We did not observe any significant difference in the expression of MCP-1 between the Beijing strain and laboratory strain, which has been shown previously [60], and did not detect difference in the expression of IFN-α. It has been suggested that Beijing strains induce more type 1 interferons [66, 67]; however, other studies have shown that IFN-α equalizes in lungs of BALB/c mice by day 14 [55], consistent with our findings. Therefore, differences in the cytokine induction between strains clearly depend on the model system studied.

We have previously shown that Mtb is pyrazinamide sensitive in the 3-D model but not standard 2-D culture [29]. Here, antibiotic sensitivity testing in the 3-D model showed that clinical isolates are significantly less susceptible to drugs than the laboratory strain, H37Rv. Bedaquiline (10 μg/ml) was ineffective against the 1471A strain and only slightly effective for 0940Y clinical isolate, and bedaquiline resistance is emerging [68–71]. This is likely due to genotypical differences between the MDR strains. Sequencing of the strains investigated revealed nonsynonymous single nucleotide polymorphism (ns-SNP) differences in multiple genes including efflux pumps and genes involved in respiration between the clinical isolates and H37Rv [11]. Whether this contributes to increased drug resistance of the clinical strains needs to be determined [72–74]. Evidently, the divergence between results from traditional sensitivity testing methods and advanced cell culture systems has widespread clinical implications, as *in vivo* Mtb is primarily within host phagocytes and under a stressed environment. For example, a synergistic effect between pyrazinamide and bedaquiline was recently highlighted by advanced imaging studies of infected human cells [49].

We investigated the response to emerging antibiotics bedaquiline and delamanid between the clinical isolate and the laboratory strain and explored the potential of verapamil in increasing efficacy. We observed that verapamil potentiates the killing effect of bedaquiline in our microsphere system, which has been previously reported in other models [25, 37, 38]. We then showed that the effect of delamanid can similarly be potentiated by verapamil, although the effect was less marked. Verapamil augmentation for each antibiotic was greater for the clinical strain in the 3-D system, indicating strain-specific differences. Verapamil may result in a cascade of events involving the inhibition of respiratory chain complexes and energy production for efflux production in mycobacteria, and therefore, the effect potentiating anti-TB drugs is indirectly increased [24]. Verapamil's mechanism of action has been proposed to be through affecting the membrane energetics of *M. tuberculosis* [75] rather than a direct bacterial efflux pump inhibition as previously believed [23, 24, 37, 38], potentially explaining why other channel blockers were ineffective in our system. Overall, the potentiating effect of verapamil on the efficacy of antibiotics within the 3-D system was marked, in particular when clinical strains were studied.

Investigation of calcium channel blockers and efflux pump inhibitors other than verapamil had no combined effect with delamanid. Within our 3-D cell culture model, transport systems will be active on three separate

membranes, the mycobacterial membrane, the phagolysosomal membrane, and the macrophage cell membrane, representing a significant experimental challenge to fully dissect underlying mechanisms. At the same time, this reflects the true complexity of events in patients. We suspect that verapamil may be enhancing the potency of delamanid by acting at all three membranes, and this additive effect leads to the overall phenotype.

In conclusion, we demonstrate that clinical and laboratory strains have significantly different virulence and antibiotic sensitivity when studied in a human 3-D cell culture system. Prolonged subculture of a clinical strain leads to attenuation, demonstrating that the system can be utilized to investigate mycobacterial pathogenic factors. Our data demonstrate that the 3-D bioelectrospray model, where gene expression reflects events in patients [27] and mirrors the critical 3-D granuloma organisation [45, 76], is an additional platform to test the effectiveness of antibiotics and identifies differences in antibiotic sensitivity and the effect of adjunctive therapy. Studying more complex assays at the preliminary drug development stage may help identify and refine optimal lead combinations.

Data Availability

All primary data is available from the corresponding author.

Conflicts of Interest

The authors declare that the research was conducted in the absence of any commercial or financial relationships that could be construed as a potential conflict of interest.

Authors' Contributions

MB, LT, and EK performed the laboratory analyses, NC and XG characterised the Mtb strains, OK supervised the micro-CT analyses, and FD and PE conceived the project and coordinated the experiments. All authors had intellectual input into the progression of the project and contributed to the manuscript writing.

Acknowledgments

We would like to thank Drs Jennifer Russell and Regina Teo, University of Southampton, for excellent technical assistance. We thank Dr Anton Page, Head of Biomedical Imaging Unit (BIU), University of Southampton, for providing support with electron scanning microscopy. This work was supported by the UK Antimicrobial Resistance Cross Council Initiative funded by the Biotechnology and Biological Sciences Research Council and the Medical Research Council (MR/N006631/1 and MR/P023754/1). We are grateful to NAMRIP (Network for Antimicrobial Resistance and Infection Prevention) for the support, including pump-priming funding via NAMRIP's EPSRC grant NAMRA (EP/M027260/1), part of the EPSRC, Network for Antimicrobial Action, "Bridging the Gap" programme. We thank the NIHR Imperial BRC for the support.

Supplementary Materials

Supplementary 1. Figure S1: clinical isolate 0414B lux and other reference strains grow more rapidly in the 3-D model. (A) H37Rv lux grows faster than the clinical isolate 0414B lux and investigated reference strains (Erdman lux and CDC1551 lux) in Middlebrook 7H9 broth measured by optical density (OD) at 600 nm. Experiments were performed in triplicate. (B) H37Rv lux is attenuated in comparison to the clinical isolate 0414B lux and the reference strains, Erdman lux and CDC1551 lux, in the 3-D system measured by luminescence. (C) Colony counts performed at day 26 confirm that H37Rv lux growth is reduced in comparison to the clinical isolate 0414B lux and the reference strains, Erdman lux and CDC1551 lux, in the 3-D system. Colour code as in (A) and (B). (B, C) Data are the mean ± standard error of the mean of an experiment performed in triplicate and are representative of two separate experiments. Statistical analyses were carried out using 2-way ANOVA with Tukey's multiple comparison test (A, B) or ordinary one-way ANOVA Tukey's multiple comparison test (C); $^{****}p < 0.0001$, $^{***}p < 0.001$, and $^{**}p < 0.01$.

Supplementary 2. Figure S2: survival of host cells at day 7. Upon infection with either H37Rv lux (black), reduced cytotoxicity compared to uninfected cells was noted by LDH release and CellTiter-Glo 3-D cell viability assay. When compared to 0414B lux (red), no difference was observed in host cell toxicity measured by CytoTox-Glo cytotoxicity assay (A) or CellTiter-Glo 3-D cell viability assay (C) between strains. Toxicity of host cells infected with H37Rv lux was significantly lower than cells infected with clinical isolate 0414B lux at day 7 when analysed by the LDH cytotoxicity assay (B). Data are mean ± SEM of 3 separate experiments. Statistics: ordinary one-way ANOVA with Tukey's multiple comparison test (A, B, C); $^{***}p < 0.001$, $^{*}p < 0.1$, and $^{ns}p > 0.05$.

Supplementary 3. Figure S3: secretion of multiple cytokines by 0414B-infected cells is reduced relative to H37Rv-infected cells. The clinical isolate 0414B lux was significantly less proinflammatory than the laboratory strain H37Rv lux. (A–F) Six significantly different cytokines in response to the two strains. (G–L) Cytokines and MMPs that were secreted were similarly upregulated in response to the two strains, analysed in the same samples by Luminex multiplex array. Uninfected PBMCs are control. Normalised data from two donors analysed in triplicate are presented (data are presented as a percentage vs. H37Rv lux strain). Statistical analyses were performed using ordinary one-way ANOVA with Tukey's multiple comparison test; $^{****}p < 0.0001$, $^{***}p < 0.001$, $^{**}p < 0.01$, $^{*}p < 0.1$, and $^{ns}p > 0.05$.

Supplementary 4. Figure S4: verapamil increases Mtb killing in 7H9 broth. Anti-TB drugs were added at day 1 to 7H9 broth and Mtb growth monitored by luminescence: bedaquiline at 5 μg/ml (BDQ 5, beige) and 10 μg/ml (BDQ 10, dark brown), verapamil at 50 μg/ml (VPL 50, light blue), and delamanid at 0.5 μg/ml (DLM 0.5, orange) and 5 μg/ml (DLM 5, light green). Verapamil alone did not affect initial

growth of Mtb and had a minimal inhibitory effect at later-time points (A–F). Bedaquiline was more effective against the clinical isolate than the laboratory strain (A, B). Verapamil's potentiating effect on bedaquiline in killing bacteria was observed at later time points for H37Rv lux (A) and minimally 0414B lux (B). Delamanid had substantial killing effect on Mtb; however, bacteria quickly recovered (B, C, E, F). The decrease in bacterial growth was potentiated by verapamil, and it was considerably greater for the clinical isolate relative to H37Rv, but bacteria revived at later time points (B, C, E, F). Mtb growth was unaffected by DMSO, used as solvent for all the compounds tested. Crosses (x) show background level of luminescence. Addition of antibiotics is specified by a black arrow. Data are mean ± SEM for an experiment performed in triplicate and representative of 2 separate experiments. Statistical analyses were done using 2-way ANOVA with Tukey's multiple comparison test; $^{****}p < 0.0001$, $^{*}p < 0.1$, and $^{ns}p > 0.05$.

Supplementary 5. Figure S5: alternative efflux pump inhibitors combined with delamanid do not have potent effect as verapamil in the 3-D system. Compounds were added at day 1 to 3-D culture and Mtb growth monitored by luminescence: delamanid at 0.5 μg/ml (DLM 0.5, orange); verapamil at 50 μg/ml (VPL 50, light blue); tariquidar at 0.5 μg/ml (TQD 0.5, light grey-green), 5 μg/ml (TQD 5, light brown), 10 μg/ml (TQD 10, dark red), and 50 μg/ml (TQD 50, dark brown); diltiazem at 5 μg/ml (DLZ 5, light blue) and 50 μg/ml (DLZ 50, midblue); amlodipine at 3 μg/ml (AML 3, bright red) and 30 μg/ml (AML 30, dark red); chlorpromazine at 2 μg/ml (CPZ 2, light green) and 20 μg/ml (CPZ 20, dark green); and carbonyl cyanide 3-chlorophenylhydrazone at 2 μg/ml (CCCP 2, lilac) and 20 μg/ml (CCCP 20, midpurple). Verapamil showed a potentiating effect on delamanid in inhibiting Mtb growth (A). Addition of tariquidar, diltiazem, or CCCP to delamanid had no effect at the concentrations tested (B, C, F). Supplementation of amlodipine with delamanid had minimal effect but only at a higher concentration used (D). Similarly, combining chlorpromazine 20 μg/ml with delamanid showed very slight Mtb killing effect (E). Higher concentrations of tariquidar and chlorpromazine applied on their own (50 μg/ml and 20 μg/ml, respectively) had some inhibitory effect on the clinical isolate (B, E). Mtb growth was unaffected by DMSO, used as solvent for all the compounds tested. Crosses (x) represent background level of luminescence. Black arrow shows antibiotic addition. Data are mean ± SEM for an experiment performed in triplicate and representative of 2 separate experiments. Statistical analyses were carried out using 2-way ANOVA with Tukey's multiple comparison test; $^{ns}p > 0.05$.

Supplementary 6. Video 1: reconstruction of micro-CT images of Mtb-infected microspheres embedded in resin. For illustrative purposes, 3 microspheres have been highlighted, with cells within spheres highlighted yellow and cellular aggregates blue. Available for review at https://eprints.soton.ac.uk/488783/.

Supplementary 7. Table S1: classification of different clinical strains and antibiotic sensitivity by reference laboratory testing. RIF: rifampicin; INH: isoniazid; PZA: pyrazinamide; EMB: ethambutol; AMIK: amikacin; CAP: caprazamycin B; MOXI: moxifloxacin; OFL: ofloxacin.

References

[1] M. Pai, T. Kasaeva, and S. Swaminathan, "Covid-19's devastating effect on tuberculosis care - a path to recovery," *The New England Journal of Medicine*, vol. 386, no. 16, pp. 1490–1493, 2022.

[2] F. Conradie, A. H. Diacon, N. Ngubane et al., "Treatment of highly drug-resistant pulmonary tuberculosis," *The New England Journal of Medicine*, vol. 382, no. 10, pp. 893–902, 2020.

[3] K. Dheda, C. E. Barry 3rd, and G. Maartens, "Tuberculosis," *Lancet*, vol. 387, no. 10024, pp. 1211–1226, 2016.

[4] V. A. Dartois and E. J. Rubin, "Anti-tuberculosis treatment strategies and drug development: challenges and priorities," *Nature Reviews. Microbiology*, vol. 20, no. 11, pp. 685–701, 2022.

[5] W. Steenken, "Lysis of tubercle bacilli *in vitro*," *Experimental Biology and Medicine*, vol. 33, no. 2, pp. 253–255, 1935.

[6] G. P. Kubica, T. H. Kim, and F. P. Dunbar, "Designation of strain H37Rv as the neotype of *Mycobacterium tuberculosis*," *International Journal of Systematic Bacteriology*, vol. 22, no. 2, pp. 99–106, 1972.

[7] N. Andreu and I. Gibert, "Cell population heterogeneity in *Mycobacterium tuberculosis* H37Rv," *Tuberculosis (Edinburgh, Scotland)*, vol. 88, no. 6, pp. 553–559, 2008.

[8] P. Domenech and M. B. Reed, "Rapid and spontaneous loss of phthiocerol dimycocerosate (PDIM) from *Mycobacterium tuberculosis* grown in vitro: implications for virulence studies," *Microbiology*, vol. 155, no. 11, pp. 3532–3543, 2009.

[9] D. Brites and S. Gagneux, "Co-evolution of Mycobacterium tuberculosis and Homo sapiens," *Immunological Reviews*, vol. 264, no. 1, pp. 6–24, 2015.

[10] M. Merker, C. Blin, S. Mona et al., "Evolutionary history and global spread of the Mycobacterium tuberculosis Beijing lineage," *Nature Genetics*, vol. 47, pp. 242–249, 2015.

[11] N. Casali, V. Nikolayevskyy, Y. Balabanova et al., "Evolution and transmission of drug-resistant tuberculosis in a Russian population," *Nature Genetics*, vol. 46, no. 3, pp. 279–286, 2014.

[12] P. Y. Khan, M. F. Franke, C. Hewison et al., "All-oral longer regimens are effective for the management of multidrug-resistant tuberculosis in high-burden settings," *The European Respiratory Journal*, vol. 59, no. 1, p. 2004345, 2022.

[13] D. F. Warner and V. Mizrahi, "Shortening treatment for tuberculosis — back to basics," *The New England Journal of Medicine*, vol. 371, no. 17, pp. 1642-1643, 2014.

[14] S. E. Dorman, P. Nahid, E. V. Kurbatova et al., "Four-month rifapentine regimens with or without moxifloxacin for tuberculosis," *The New England Journal of Medicine*, vol. 384, no. 18, pp. 1705–1718, 2021.

[15] A. J. Nunn, P. P. J. Phillips, S. K. Meredith et al., "A trial of a shorter regimen for rifampin-resistant tuberculosis," *The New England Journal of Medicine*, vol. 380, no. 13, pp. 1201–1213, 2019.

[16] E. De Rossi, J. A. Aínsa, and G. Riccardi, "Role of mycobacterial efflux transporters in drug resistance: an unresolved

question," *FEMS Microbiology Reviews*, vol. 30, no. 1, pp. 36–52, 2006.

[17] G. E. Louw, R. M. Warren, N. C. Gey van Pittius et al., "Rifampicin reduces susceptibility to ofloxacin in rifampicin-resistant *Mycobacterium tuberculosis* through efflux," *American Journal of Respiratory and Critical Care Medicine*, vol. 184, no. 2, pp. 269–276, 2011.

[18] R. P. Morris, L. Nguyen, J. Gatfield et al., "Ancestral antibiotic resistance in *Mycobacterium tuberculosis*," *Proceedings of the National Academy of Sciences of the United States of America*, vol. 102, no. 34, pp. 12200–12205, 2005.

[19] L. Nguyen and C. J. Thompson, "Foundations of antibiotic resistance in bacterial physiology: the mycobacterial paradigm," *Trends in Microbiology*, vol. 14, no. 7, pp. 304–312, 2006.

[20] L. J. V. Piddock, "Multidrug-resistance efflux pumps - not just for resistance," *Nature Reviews. Microbiology*, vol. 4, no. 8, pp. 629–636, 2006.

[21] K. N. Adams, K. Takaki, L. E. Connolly et al., "Drug tolerance in replicating mycobacteria mediated by a macrophage-induced efflux mechanism," *Cell*, vol. 145, no. 1, pp. 39–53, 2011.

[22] K. N. Adams, J. D. Szumowski, and L. Ramakrishnan, "Verapamil, and its metabolite norverapamil, inhibit macrophage-induced, bacterial efflux pump-mediated tolerance to multiple anti-tubercular drugs," *The Journal of Infectious Diseases*, vol. 210, no. 3, pp. 456–466, 2014.

[23] S. Gupta, S. Tyagi, D. V. Almeida, M. C. Maiga, N. C. Ammerman, and W. R. Bishai, "Acceleration of tuberculosis treatment by adjunctive therapy with verapamil as an efflux inhibitor," *American Journal of Respiratory and Critical Care Medicine*, vol. 188, no. 5, pp. 600–607, 2013.

[24] D. Machado, D. Pires, J. Perdigão et al., "Ion channel blockers as antimicrobial agents, efflux inhibitors, and enhancers of macrophage killing activity against drug resistant *Mycobacterium tuberculosis*," *PLoS One*, vol. 11, no. 2, article e0149326, 2016.

[25] H. Ghajavand, M. Kargarpour Kamakoli, S. Khanipour et al., "High prevalence of bedaquiline resistance in treatment-naive tuberculosis patients and verapamil effectiveness," *Antimicrobial Agents and Chemotherapy*, vol. 63, no. 3, 2019.

[26] L. B. Tezera, M. K. Bielecka, A. Chancellor et al., "Dissection of the host-pathogen interaction in human tuberculosis using a bioengineered 3-dimensional model," *eLife*, vol. 6, 2017.

[27] M. T. Reichmann, L. B. Tezera, A. F. Vallejo et al., "Integrated transcriptomic analysis of human tuberculosis granulomas and a biomimetic model identifies therapeutic targets," *The Journal of Clinical Investigation*, vol. 131, no. 15, article e148136, 2021.

[28] P. Elkington, M. E. Polak, M. T. Reichmann, and A. Leslie, "Understanding the tuberculosis granuloma: the matrix revolutions," *Trends in Molecular Medicine*, vol. 28, no. 2, pp. 143–154, 2022.

[29] M. K. Bielecka, L. B. Tezera, R. Zmijan et al., "A bioengineered three-dimensional cell culture platform integrated with microfluidics to address antimicrobial resistance in tuberculosis," *MBio*, vol. 8, no. 1, article e02073, 2017.

[30] N. Andreu, A. Zelmer, T. Fletcher et al., "Optimisation of bioluminescent reporters for use with mycobacteria," *PLoS One*, vol. 5, no. 5, article e10777, 2010.

[31] T. Parish and N. G. Stoker, "Electroporation of mycobacteria," *Methods in Molecular Biology*, vol. 101, pp. 129–144, 1998.

[32] L. B. Tezera, M. K. Bielecka, and P. T. Elkington, "Bioelectrospray methodology for dissection of the host-pathogen interaction in human tuberculosis," *Bio-Protocol*, vol. 7, no. 14, 2017.

[33] V. L. Workman, L. B. Tezera, P. T. Elkington, and S. N. Jayasinghe, "Controlled generation of microspheres incorporating extracellular matrix fibrils for three-dimensional cell culture," *Advanced Functional Materials*, vol. 24, no. 18, pp. 2648–2657, 2014.

[34] P. T. Elkington, J. A. Green, and J. S. Friedland, "Filter sterilization of highly infectious samples to prevent false negative analysis of matrix metalloproteinase activity," *Journal of Immunological Methods*, vol. 309, no. 1-2, pp. 115–119, 2006.

[35] L. B. Tezera, M. K. Bielecka, P. Ogongo et al., "Anti-PD-1 immunotherapy leads to tuberculosis reactivation via dysregulation of TNF-α," *eLife*, vol. 9, 2020.

[36] S. Khoshnood, E. Taki, N. Sadeghifard et al., "Mechanism of action, resistance, synergism, and clinical implications of delamanid against multidrug-resistant Mycobacterium tuberculosis," *Frontiers in Microbiology*, vol. 12, article 717045, 2021.

[37] S. Gupta, K. A. Cohen, K. Winglee, M. Maiga, B. Diarra, and W. R. Bishai, "Efflux inhibition with verapamil potentiates bedaquiline in *Mycobacterium tuberculosis*," *Antimicrobial Agents and Chemotherapy*, vol. 58, no. 1, pp. 574–576, 2014.

[38] S. Gupta, S. Tyagi, and W. R. Bishai, "Verapamil increases the bactericidal activity of bedaquiline against *Mycobacterium tuberculosis* in a mouse model," *Antimicrobial Agents and Chemotherapy*, vol. 59, no. 1, pp. 673–676, 2015.

[39] P. Kannan, S. Telu, S. Shukla et al., "The "specific" P-glycoprotein inhibitor tariquidar is also a substrate and an inhibitor for breast cancer resistance protein (BCRP/ABCG2)," *ACS Chemical Neuroscience*, vol. 2, no. 2, pp. 82–89, 2011.

[40] E. A. Weinstein, T. Yano, L. S. Li et al., "Inhibitors of type II NADH: menaquinone oxidoreductase represent a class of antitubercular drugs," *Proceedings of the National Academy of Sciences of the United States of America*, vol. 102, no. 12, pp. 4548–4553, 2005.

[41] P. G. Heytler and W. W. Prichard, "A new class of uncoupling agents — carbonyl cyanide phenylhydrazones," *Biochem Biophys Res Commun*, vol. 7, no. 4, pp. 272–275, 1962.

[42] J. Kasianowicz, R. Benz, and S. McLaughlin, "The kinetic mechanism by which CCCP (carbonyl cyanide m-chlorophenylhydrazone) transports protons across membranes," *J Membr Biol*, vol. 82, no. 2, pp. 179–190, 1984.

[43] V. Dartois and C. E. Barry 3rd., "A medicinal chemists' guide to the unique difficulties of lead optimization for tuberculosis," *Bioorganic & Medicinal Chemistry Letters*, vol. 23, no. 17, pp. 4741–4750, 2013.

[44] B. Prideaux, L. E. Via, M. D. Zimmerman et al., "The association between sterilizing activity and drug distribution into tuberculosis lesions," *Nature Medicine*, vol. 21, no. 10, pp. 1223–1227, 2015.

[45] E. F. McCaffrey, M. Donato, L. Keren et al., "The immunoregulatory landscape of human tuberculosis granulomas," *Nature Immunology*, vol. 23, no. 2, pp. 318–329, 2022.

[46] S. Stergiopoulos, S. B. Calvert, C. A. Brown et al., "Cost drivers of a hospital-acquired bacterial pneumonia and ventilator-associated bacterial pneumonia phase 3 clinical trial," *Clinical Infectious Diseases*, vol. 66, no. 1, pp. 72–80, 2018.

[47] M. K. Bielecka and P. Elkington, "Advanced cellular systems to study tuberculosis treatment," *Current Opinion in Pharmacology*, vol. 42, pp. 16–21, 2018.

[48] B. B. Aldridge, D. Barros-Aguirre, C. E. Barry 3rd et al., "The tuberculosis drug accelerator at year 10: what have we learned?," *Nature Medicine*, vol. 27, pp. 1333–1337, 2021.

[49] P. Santucci, D. J. Greenwood, A. Fearns, K. Chen, H. Jiang, and M. G. Gutierrez, "Intracellular localisation of Mycobacterium tuberculosis affects efficacy of the antibiotic pyrazinamide," *Nature Communications*, vol. 12, no. 1, p. 3816, 2021.

[50] S. Borrell, A. Trauner, D. Brites et al., "Reference set of Mycobacterium tuberculosis clinical strains: a tool for research and product development," *PLoS One*, vol. 14, no. 3, article e0214088, 2019.

[51] T. R. Ioerger, Y. Feng, K. Ganesula et al., "Variation among genome sequences of H37Rv strains of *Mycobacterium tuberculosis* from multiple laboratories," *Journal of Bacteriology*, vol. 192, no. 14, pp. 3645–3653, 2010.

[52] C. A. Molina-Torres, J. Castro-Garza, J. Ocampo-Candiani, M. Monot, S. T. Cole, and L. Vera-Cabrera, "Effect of serial subculturing on the genetic composition and cytotoxic activity of *Mycobacterium tuberculosis*," *Journal of Medical Microbiology*, vol. 59, no. 4, pp. 384–391, 2010.

[53] P. Elkington, M. Lerm, N. Kapoor et al., "In vitro granuloma models of tuberculosis: potential and challenges," *The Journal of Infectious Diseases*, vol. 219, no. 12, pp. 1858–1866, 2019.

[54] R. Sarkar, L. Lenders, K. A. Wilkinson, R. J. Wilkinson, and M. P. Nicol, "Modern lineages of *Mycobacterium tuberculosis* exhibit lineage-specific patterns of growth and cytokine induction in human monocyte-derived macrophages," *PLoS One*, vol. 7, no. 8, article e43170, 2012.

[55] B. Lopez, D. Aguilar, H. Orozco et al., "A marked difference in pathogenesis and immune response induced by different *Mycobacterium tuberculosis* genotypes," *Clinical and Experimental Immunology*, vol. 133, no. 1, pp. 30–37, 2003.

[56] Q. Li, C. C. Whalen, J. M. Albert et al., "Differences in rate and variability of intracellular growth of a panel of *Mycobacterium tuberculosis* clinical isolates within a human monocyte model," *Infection and Immunity*, vol. 70, no. 11, pp. 6489–6493, 2002.

[57] S. A. Theus, M. D. Cave, and K. D. Eisenach, "Intracellular macrophage growth rates and cytokine profiles of *Mycobacterium tuberculosis* strains with different transmission dynamics," *The Journal of Infectious Diseases*, vol. 191, no. 3, pp. 453–460, 2005.

[58] M. Zhang, J. Gong, Z. Yang, B. Samten, M. D. Cave, and P. F. Barnes, "Enhanced capacity of a widespread strain of *Mycobacterium tuberculosis* to grow in human macrophages," *The Journal of Infectious Diseases*, vol. 179, no. 5, pp. 1213–1217, 1999.

[59] B. S. Zha, L. Desvignes, T. J. Fergus et al., "Bacterial strain-dependent dissociation of cell recruitment and cell-to-cell spread in early M. tuberculosis infection," *MBio*, vol. 13, no. 3, article e0133222, 2022.

[60] G. Huet, P. Constant, W. Malaga et al., "A lipid profile typifies the Beijing strains of *Mycobacterium tuberculosis*: identification of a mutation responsible for a modification of the structures of phthiocerol dimycocerosates and phenolic glycolipids," *The Journal of Biological Chemistry*, vol. 284, no. 40, pp. 27101–27113, 2009.

[61] N. Rakotosamimanana, V. Raharimanga, S. F. Andriamandimby et al., "Variation in gamma interferon responses to different infecting strains of *Mycobacterium tuberculosis* in acid-fast bacillus smear-positive patients and household contacts in Antananarivo, Madagascar," *Clinical and Vaccine Immunology*, vol. 17, no. 7, pp. 1094–1103, 2010.

[62] M. B. Reed, P. Domenech, C. Manca et al., "A glycolipid of hypervirulent tuberculosis strains that inhibits the innate immune response," *Nature*, vol. 431, no. 7004, pp. 84–87, 2004.

[63] H. Sohn, K. S. Lee, S. Y. Kim et al., "Induction of cell death in human macrophages by a highly virulent Korean isolate of *Mycobacterium tuberculosis* and the virulent strain H37Rv," *Scandinavian Journal of Immunology*, vol. 69, no. 1, pp. 43–50, 2009.

[64] M. Tanveer, Z. Hasan, A. Kanji, R. Hussain, and R. Hasan, "Reduced TNF-alpha and IFN-gamma responses to Central Asian strain 1 and Beijing isolates of *Mycobacterium tuberculosis* in comparison with H37Rv strain," *Transactions of the Royal Society of Tropical Medicine and Hygiene*, vol. 103, no. 6, pp. 581–587, 2009.

[65] C. Wang, P. Peyron, O. Mestre et al., "Innate immune response to *Mycobacterium tuberculosis* Beijing and other genotypes," *PLoS One*, vol. 5, no. 10, article e13594, 2010.

[66] C. Manca, L. Tsenova, A. Bergtold et al., "Virulence of a *Mycobacterium tuberculosis* clinical isolate in mice is determined by failure to induce Th1 type immunity and is associated with induction of IFN-alpha/beta," *Proceedings of the National Academy of Sciences of the United States of America*, vol. 98, no. 10, pp. 5752–5757, 2001.

[67] C. Manca, L. Tsenova, S. Freeman et al., "Hypervirulent *M. tuberculosis* W/Beijing strains upregulate type I IFNs and increase expression of negative regulators of the Jak-Stat pathway," *Journal of Interferon & Cytokine Research*, vol. 25, no. 11, pp. 694–701, 2005.

[68] G. Degiacomi, J. C. Sammartino, V. Sinigiani, P. Marra, A. Urbani, and M. R. Pasca, "In vitro study of bedaquiline resistance in Mycobacterium tuberculosis multi-drug resistant clinical isolates," *Frontiers in Microbiology*, vol. 11, article 559469, 2020.

[69] N. A. Ismail, S. V. Omar, H. Moultrie et al., "Assessment of epidemiological and genetic characteristics and clinical outcomes of resistance to bedaquiline in patients treated for rifampicin-resistant tuberculosis: a cross-sectional and longitudinal study," *The Lancet Infectious Diseases*, vol. 22, no. 4, pp. 496–506, 2022.

[70] K. Kaniga, R. Hasan, R. Jou et al., "Bedaquiline drug resistance emergence assessment in multidrug-resistant tuberculosis (MDR-TB): a 5-year prospective in vitro surveillance study of bedaquiline and other second-line drug susceptibility testing in MDR-TB isolates," *Journal of Clinical Microbiology*, vol. 60, article e0291920, 2022.

[71] S. H. Wu, H. H. Chan, H. C. Hsiao, and R. Jou, "Primary bedaquiline resistance among cases of drug-resistant tuberculosis in Taiwan," *Frontiers in Microbiology*, vol. 12, article 754249, 2021.

[72] K. Andries, C. Villellas, N. Coeck et al., "Acquired resistance of *Mycobacterium tuberculosis* to bedaquiline," *PLoS One*, vol. 9, no. 7, article e102135, 2014.

[73] A. Kanji, R. Hasan, A. Ali et al., "Single nucleotide polymorphisms in efflux pumps genes in extensively drug resistant *Mycobacterium tuberculosis* isolates from Pakistan," *Tuberculosis (Edinburgh, Scotland)*, vol. 107, pp. 20–30, 2017.

[74] J. Liu, W. Shi, S. Zhang et al., "Mutations in efflux pump Rv1258c (Tap) cause resistance to pyrazinamide, isoniazid, and streptomycin in *M. tuberculosis*," *Frontiers in Microbiology*, vol. 10, p. 216, 2019.

[75] C. Chen, S. Gardete, R. S. Jansen et al., "Verapamil targets membrane energetics in *Mycobacterium tuberculosis*," *Antimicrobial Agents and Chemotherapy*, vol. 62, no. 5, 2018.

[76] H. P. Gideon, T. K. Hughes, C. N. Tzouanas et al., "Multimodal profiling of lung granulomas in macaques reveals cellular correlates of tuberculosis control," *Immunity*, vol. 55, pp. 827–846.e810, 2022.